Chi Zhang[1,2,3], Yoshifumi Futaana[3], Hans Nilsson[3], Zhaojin Rong[1,2], Moa Persson[4], Lucy Klinger[5], Xiaodong Wang[3], Gabriella Stenberg Wieser[3], Stas Barabash[3], Chuanfei Dong[6], Mats Holmström[3], and Yong Wei[1,2]

[1]Key Laboratory of Earth and Planetary Physics, Institute of Geology and Geophysics, Chinese Academy of Sciences, Beijing, China

[2] College of Earth and Planetary Sciences, University of Chinese Academy of Sciences, Beijing, China

[3]Swedish Institute of Space Physics, Kiruna, Sweden

[4] IRAP, CNRS-UPS-CNES, Toulouse, France

[5]Beijing International Center for Mathematical Research, Peking University, Beijing, China

[6]Princeton Plasma Physics Laboratory and Department of Astrophysical Sciences, Princeton University, Princeton, NJ, USA

***Corresponding author**: Chi Zhang (zhangchi@mail.iggcas.ac.cn)

Key Points:

- Sunward ion flows in the tail occur more frequently and with a higher flow flux during solar maximum
- Sunward flows do not significantly reduce the total heavy ion escape at Mars
- A strong correlation between crustal fields and sunward flow is identified

Abstract

We investigate sunward planetary ions in the Martian magnetotail that potentially reduce the amount of escaping ions. The global properties of sunward flows in the Martian magnetotail are characterized, based on over 13-years of ion data (May 2007–December 2020) collected by the ASPERA-3 instrument on Mars Express. We find that sunward flows mainly occur in the vicinity of the crustal fields, implying that crustal fields may play a key role in producing such flows. The occurrence rate and sunward flux are higher during solar maximum rather than solar minimum. However, we identify a relatively low occurrence rate of sunward flows and low sunward flux, suggesting that sunward flows have negligible influence on total ion escape at Mars. This is different from those at Venus, where sunward flows can significantly decrease the total escape rates of ions.

Plain Language Summary

Without the protection of an intrinsic magnetic field, solar wind can interact directly with the Martian atmosphere and drive ion escape, which plays a vital role in the evolution of the planetary atmosphere. It was shown that, on average, all Martian ions accelerated by the solar wind flow downstream and escape

to interplanetary space. However, some planetary ions can flow sunward or planetward, possibly reducing total ion escape. The mechanism and role of these sunward ions remain unclear. Here, we present a statistical analysis that reveals the global properties of sunward flows at Mars based on over 13 years of Mars Express data. Our results suggest that crustal fields may play a role in driving sunward flows. We also show that sunward flows cannot significantly reduce the escaping flux of Martian atmospheric ions to space regardless of solar activity. This finding can help us understand ion escape and tail dynamics at Mars.

1 Introduction

It is widely accepted that solar wind interaction with Mars is a critical factor in atmosphere removal. The lack of global intrinsic magnetic fields allows solar wind to directly interact with the Martian atmosphere and scavenge the planetary ions to escape away [e.g., Lundin et al., 1989; Barabash et al., 2007; Dong et al., 2014, 2015]. As it approaches Mars, the solar wind flow, which carries a "frozen-in" interplanetary magnetic field (IMF), will decelerate upon interaction with the Martian ionosphere, resulting in an induced magnetosphere [e.g., Futaana et al., 2017; Luhmann et al., 2004; Ma et al., 2002; Zhang et al., 2022]. Correspondingly, the solar wind accelerates planetary ions via the Lorenz force, which is exerted by the electromagnetic fields, such as motional electric fields [Barabash et al. 1991; Dong et al. 2015; Fang et al., 2008], Hall electric fields [Dubinin et al. 2011; Lundin, 2011], and ambipolar electric fields [e.g. Collinson et al. 2019; Xu et al. 2021; Ma et al., 2019]. In addition, localized intense crustal fields complexify the Martian magnetosphere and affect ion escape [e.g., Connerney et al., 2005; Fang et al., 2010; Ramstad et al., 2016; Zhang et al., 2021].

The motion of Martian ions show that they are accelerated by solar wind, on average, will flow downstream or tailward and eventually escape into interplanetary space [Nilsson et al., 2012; Fränz et al., 2015]. Nonetheless, not all planetary ions flow downstream.

For Venus, which also possesses an induced magnetosphere owing to the interaction between solar wind and its ionosphere, previous studies have reported on the presence of sunward ions in the induced magnetotail, which probably reduce ion escape [e.g., Dubinin et al., 2012, 2013; Lundin, 2011; Kollmann et al., 2016; Persson et al., 2018, 2020]. In these studies, sunward flows are also referred to as "planetward flows" or "return flows". Furthermore, Kollmann et al. [2016], Persson et al. [2018] and Masunaga et al. [2019] found that the occurrence rate of sunward flows and the total sunward flux seems to increase from solar minimum to solar maximum, leading to a decrease in the total net escape rate of heavy ions at solar maximum. This indicates that sunward flows can significantly impact the ion escape at Venus and its atmospheric evolution [Persson et al., 2020].

For Mars, the sunward ions (or planetward flows) in the Martian current sheet

were observed and can be explained by magnetic reconnection [Harada et al., 2015a, 2015b, 2017, 2020]. However, these studies only concern the planetward flux or flow in the current sheet. Therefore, the global properties of sunward flows in the Martian magnetotail are still not completely understood. The key question is whether sunward flows significantly reduce ion escape at Mars as they do at Venus. The relationship between sunward flows, solar wind conditions, and crustal fields are still unclear. Targeting these problems, we utilize a dataset of long period ions data measured by Mars Express (MEX) to reveal the global properties of sunward flows, their effects on ion escape, their variation in the solar cycle, and their comparison to Venusian sunward flows. Studying these flows is beneficial to understanding the tail dynamics and the evolution of the Martian atmosphere.

2 Datasets and Coordinates

In this study, we used the dataset of long period of ion data (2007.5–2020.12) as measured by the Ion Mass Analyzer (IMA), which is part of the Analyzer of Space Plasma and Energetic Atoms (ASPERA-3) instrument package on Mars Express (MEX) [Barabash et al., 2006]. The intrinsic elevation-azimuth field of view (FOV) of IMA is $4.5^{\circ} \times 360^{\circ}$. By stepping the deflection voltage for 16 steps in the entrance deflection system, IMA expands the elevation to $\pm 45°$ and the FOV to $90^{\circ} \times 360^{\circ}$, obtaining a partial three-dimensional particle distribution. After passing through the entrance deflection system, the ions enter the top hat electrostatic energy analyzer (ESA), which measures 96 different energy levels in 12s increments with a 7% energy resolution. Therefore, a full elevation sweep of 16 steps takes 192s (16 steps $\times$ 12s). Before May 2007, the energy range was 30 eV to 32 keV. From May 2007 to November 2009, the range was 10 eV to 25 keV. After November 2009, the energy range was 1 eV to 15 keV.

Ions of different masses can be separated in the magnetic deflection system due to the mass-per-charge (M/q) -dependent gyroradius. Detection of particles is made by micro-channel plates (MCPs) with anodes divided into 32 radial positions, corresponding to 32 mass channels. In addition, the MCPs are also divided into 16 sectors of 22.5°, which records the azimuthal direction of ions. Therefore, a full ion distribution consists of 32 mass channels $\times$ 96 energy steps $\times$ 16 azimuthal directions$\times$ 16 elevation directions.

We use Mars Solar Orbital (MSO) coordinates here, where $\overrightarrow{X}_{\mathrm{MSO}}$ points from Mars to the Sun, $\overrightarrow{Y}_{\mathrm{MSO}}$ points opposite to Mars' orbital velocity, and $\overrightarrow{Z}_{\mathrm{MSO}}$ completes the right-handed system.

3 Method

3.1 Moment Calculation

To study sunward flows, we mainly use moment data based on the 3D velocity distribution of ions. It is necessary to remove the noise before the moment calculation, the first of which is the "proton ghost." Part of the H^{+} deflected by the magnetic field of the mass determination will hit the surface of magnets and

subsequently scatter and cause a signal on a broad range of mass channels, a signal which is referred to as "ghost" and which can affect the moment calculation for heavy ions [e.g., Fedorov et al., 2011]. In addition to this "ghost," solar ultraviolet (UV), and the Mars Advanced Radar for Subsurface and Ionosphere Sounding (MARSIS) which was onboard the Mars Express, affect ion measurements [Voshchepynets et al., 2018]. In this study, we have removed all known types of "ghost" and other noise contaminations by following the same method in Nilsson et al. [2010, 2011, 2012, 2021].

After this, we apply the multispecies fitting technique to separate the distribution of different species (e.g., H^+, He^{2+}, O^+, and $O_2{}^+$). This method, based on fitting a Gaussian distribution function for each species, was discussed and successfully applied for IMA data [Rojas-Castillo et al., 2018]. Figure 3 in Rojas-Castillo et al. [2018] shows how it can be used to separate different species.

Each ion detected by IMA can be represented in a distribution function in phase space, $f(\vec{V})$, where $\vec{V} = (V_x,\ V_y,\ V_z)$ represents the particle's velocity. $f(\vec{V})$ can be written in terms of the measured differential particle flux and energy:

(1)

where m is the particle's mass, E is particle's energy, and the differential number flux (J) is a function of energy and the solid angle [e.g., Fränz et al., 2007]. We can then calculate the density and velocity through the plasma moments, defined as:

(2)

Therefore, the density, 0^{th} moment (k=0) can be written as:

(3)

In the spherical coordinates of IMA, it can be rewritten as:

(4)

where θ, ϕ are the elevation and azimuth angles, respectively. The elevation angle corresponds to an angle between the particle's velocity and XY_{IMA} plane; for example, $\theta = 90(-90)^\circ$ is the $+\vec{Z}_{\text{IMA}}$ ($-\vec{Z}_{\text{IMA}}$), while $\theta = 0^\circ$ represents the XY_{IMA} plane. The azimuth angle ϕ is in the XY_{IMA} plane, opening from $+\vec{X}_{\text{IMA}}$ with a positive right-hand rotation at $+\vec{Z}_{\text{IMA}}$. V_m represents the ion's speed, calculated by $V_m = \sqrt{2E_m/m}$.

Similarly, we can find the flux of each direction from 1^{st} moment:

(5)

Therefore, the velocity of particles in IMA frame can be obtained:

(6)

Finally, we convert the velocity into an MSO frame and correct for spacecraft velocity.

In order to obtain a reliable velocity, we calculate moments based on ions with energy higher than 50 eV. The first reason for this is that low-energy ions (E<50 eV) might be influenced by spacecraft potential. Both the ions' energy and the viewing direction will be changed and distorted when the ion energy is less than twice the spacecraft potential [Bergman et al., 2020]. The typical potential of MEX is lower than 10 V [Fränz et al., 2006], which indicates that our moment data of ions with an E>50eV is reliable. The second reason is that the entrance deflection system voltage is set to as close to zero deflection as possible for low-energy ions (E<50eV), resulting in a narrow field-of-view (FOV); and since only two-dimensional distribution is measured for low-energy ions, the ion moment calculation is incomplete. Using measurements above 50 eV results in moments that are incomplete in energy, but in a well-defined and predictable manner. A similar study using the lower energy (E<50 eV) data is reserved for a further study.

3.2 Selecting Criteria of the Sunward Flows

We set the following selection criteria to find the sunward flows events:

1. The spatial region we survey is the magnetotail, that is, $X_{MSO}<0$ and $R_{MSO} = \sqrt{Y_{MSO}^2 + Z_{MSO}^2} < R_{MPB}$, where ($X_{MSO}$, Y_{MSO}, Z_{MSO}) represent the position of MEX. R_{MPB} represents the radial position of the magnetic pile-up boundary (MPB) from the model of Trotignon et al. [2006].

2. To guarantee that the ions are well resolved by IMA, particularly in the Sun and tail direction (which are important for evaluating the sunward flows), we only include the data when the elevation angle of the Sun and anti-Sun directions are within the FOV of IMA frame, meaning $|\theta_{Sun}| < 45^{\circ}, |\theta_{anti-Sun}| < 45^{\circ}$, where θ_{Sun} represents the elevation angle of Sunward direction while $\theta_{anti-sun}$ represents the elevation angle of anti-Sunward direction in IMA frame. This step helps us at least to obtain a reliable estimate of the Vx component of ions.

3. We select sunward flow events from our dataset, which means that the bulk velocity of O^+ or $O_2{}^+$ is sunward, that is, Vx>0.

4. Due to the spacecraft blockage in the FOV of the IMA, we visually inspected the FOV of each event that fulfilled the above criteria and selected the reliable cases.

4. Case Study

We briefly examine a typical sunward flow case that occurred during 06:20–08:00 on February 11, 2016.

Figure 1 shows an overview of the event. Figure 1a and 1b show the trajectory of MEX projected onto the XR_{MSO} plane and the YZ_{MSO} plane (red line), where R_{MSO} is calculated by $R_{MSO} = \sqrt{(Y_{MSO}^2 + Z_{MSO}^2)}$. As shown in the energy-time spectrogram of electrons (Figure 1c) and H^+ (Figure 1d), MEX

first detected the upstream solar wind and subsequently crossed the bow shock (BS) at ~06:15 into the magnetosheath, which was identified by the appearance of heated electrons. MEX then crossed the magnetic pile-up boundary (MPB) and entered the magnetosphere at ~06:58, characterized by a decrease in heated electrons (Figure 1c) and proton flux (Figure 1d). After about 30 minutes, MEX crossed the outbound MPB at 07:22. We indicate these boundary crossings with black vertical lines in Figure 1. The outbound BS crossing, however, is hard to identify from the spectrum of electrons due to strong wave activity.

This event occurred during 07:02:56–07:06:08, when MEX was located at (–0.8, 0.77, 0.15) Rm (Rm=3396km, Mars radius) with an altitude of 395 km (see the red-shaded region in Figure 1c–1h), which was within the Martian magnetotail. During this period, MEX measured heated heavy ions (Figure 1e, 1f) with an energy range from 10 eV to 200 eV. The bulk velocity of both O^+ and $O_2{}^+$ were sunward (Figure 1g), implying that they were returning towards Mars.

We plotted the angular distribution of O+, $O_2{}^+$ in IMA frame to check the reliability of the bulk velocity and studied the ions' motion in more detail (see Figure 1i, 1j). The shaded region is the FOV of the IMA during this event. We found that the main populations of O^+ and $O_2{}^+$ are within the FOV, implying that the ion distribution was resolved. Therefore, this event meets all criteria in Section 3.2 and can be regarded as a sunward flow event.

Through inspection of the angular distribution, we find that O^+ consists of two populations, one sunward-moving and the other tailward-moving. The flux of the sunward population is higher than the tailward part, leading to a net sunward bulk velocity of O^+. Meanwhile, $O_2{}^+$ shows a similar distribution to O^+, but counts of the tailward part are fewer than O^+. The bulk velocity of O^+ and $O_2{}^+$ are basically identical, suggesting ions of both species were moving together (Figure 1g).

Of particular interest here is that this event occurred around crustal fields, which have enhanced magnetic field strength, as calculated by the Martian crustal fields model (Figure 1h) [Gao et al., 2021]. This suggests that crustal fields might play a key role in driving sunward flow, a possibility we consider in Section 5.2.

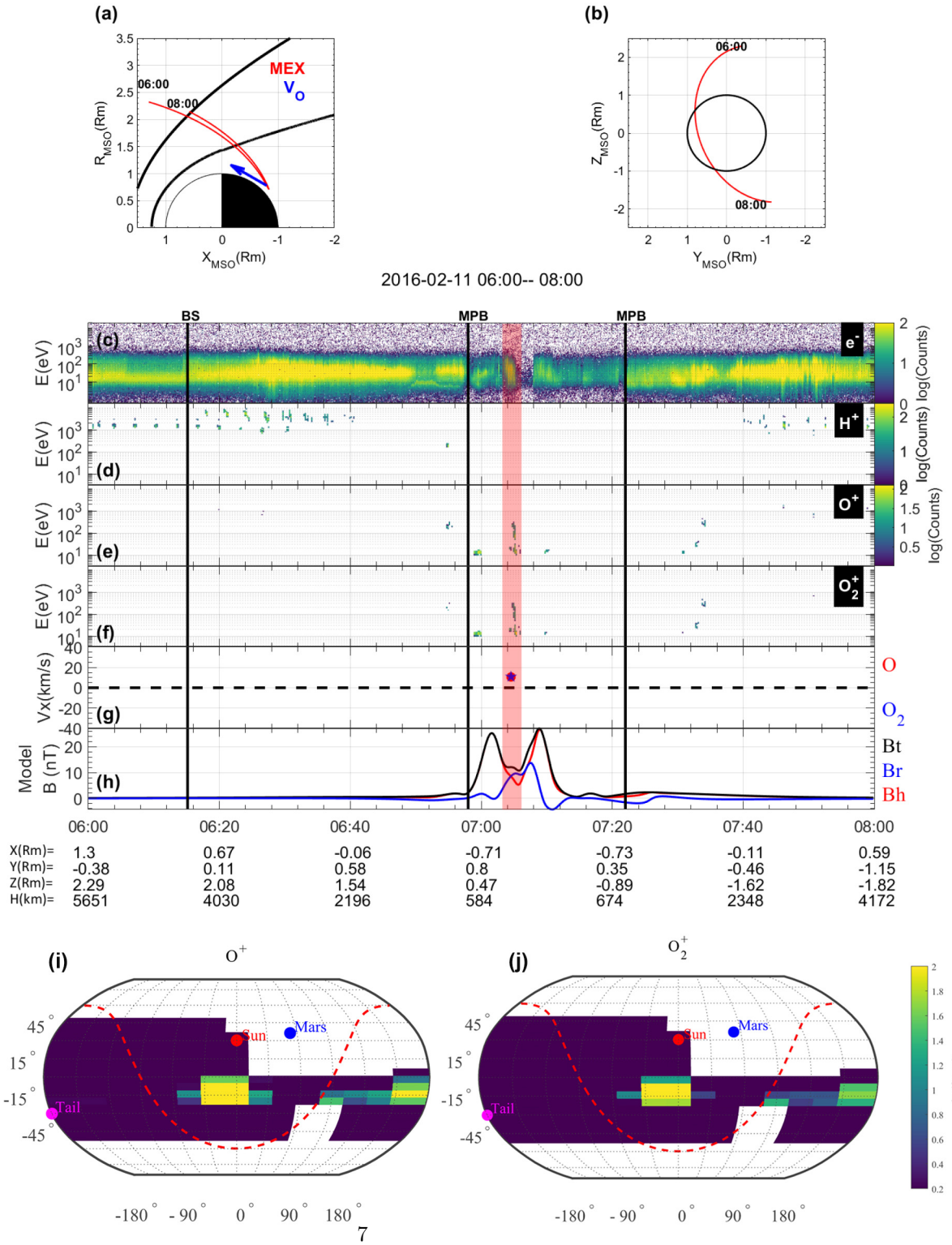
(a)
(b)
MEX
V_O
06:00
08:00
R_{MSO}(Rm)
X_{MSO}(Rm)
Z_{MSO}(Rm)
Y_{MSO}(Rm)
2016-02-11 06:00-- 08:00
BS
MPB
MPB
(c)
(d)
(e)
(f)
(g)
(h)
E(eV)
Vx(km/s)
Model B (nT)
e^-
H^+
O^+
O_2^+
log(Counts)
O
O_2
Bt
Br
Bh
06:00
06:20
06:40
07:00
07:20
07:40
08:00
X(Rm)= 1.3 0.67 -0.06 -0.71 -0.73 -0.11 0.59
Y(Rm)= -0.38 0.11 0.58 0.8 0.35 -0.46 -1.15
Z(Rm)= 2.29 2.08 1.54 0.47 -0.89 -1.62 -1.82
H(km)= 5651 4030 2196 584 674 2348 4172
(i)
(j)
O^+
O_2^+
Sun
Mars
Tail
45°
15°
-15°
-45°
-180° -90° 0° 90° 180°
log(Counts)

Figure 1. Overview of the typical sunward flow events that occurred during 06:20–08:00 on February 11, 2016. (a–b) MEX orbital trajectory during this event (red lines). Views are shown (a) in the XR plane, and (b) in the YZ plane. The black curves in (a) denote the nominal BS and MPB using the model in Trotignon et al. [2006]. The blue arrow is the bulk velocity direction of sunward O^+. The energy spectrum of electrons is shown in (c), for H+ in (d), O^+ in (e), and $O_2{}^+$ in (f). (g) shows the Vx of O^+ and $O_2{}^+$. (h) is the horizontal (red line), radial (blue line), the magnitude of magnetic fields calculated by the crustal fields model [Gao et al., 2021]. The black vertical lines denote the crossing of BS or MPB. (i) and (j) display the angular distribution of O^+ and $O_2{}^+$ in the IMA frame respectively. The red dashed lines in (i) and (j) represent the boundary that separates sunward and tailward flow.

For this event, the net sunward flux of O^+ and $O_2{}^+$ is about 6.4×10^5 $cm^{-2}s^{-1}$ and 4.8×10^5 $cm^{-2}s^{-1}$ respectively, which is about one order of magnitude lower than the average observed escape flux in the magnetotail (on the order of 10^6 $cm^{-2}s^{-1}$) [e.g. Nilsson et al., 2011, 2021; Brain et al., 2015; Inui et al., 2019].

1. Statistical Results

To draw a global picture that surveys the properties of Martian sunward flows, we conducted a statistical analysis of sunward flow events based on over 13 years of IMA data, measured from May 2007 to December 2020. We found 98 events of sunward O^+ and 134 events of sunward $O_2{}^+$ based on the criteria listed in section 3.2. The period of each event was less than 6 minutes, and only one data point of bulk velocity that corresponded to each event could be derived. Note that sunward flows are different from the nightside heavy ions precipitations studied by Diéval et al. [2013] and Hara et al. [2018], in which only the sunward flux in low-altitude ionosphere (<350km) was considered.

1. **Spatial Distribution in MSO Frame**

Figures 2a and 2b show maps of the total number of data points with a determined bulk velocity of O^+ and $O_2{}^+$ respectively in each bin with a size of 0.2Rm×0.2Rm. A major part of the data for both O^+ and $O_2{}^+$ is located in the terminator region, due to a bias in the selection criteria, where the IMA attitude should provide the Sunward and anti-Sunward directions inside the FOV (see Section 3.2), and is therefore more probable in the terminator region. Still, we have significant coverage of the entire tail up to 2.5 R_M downstream from the tail.

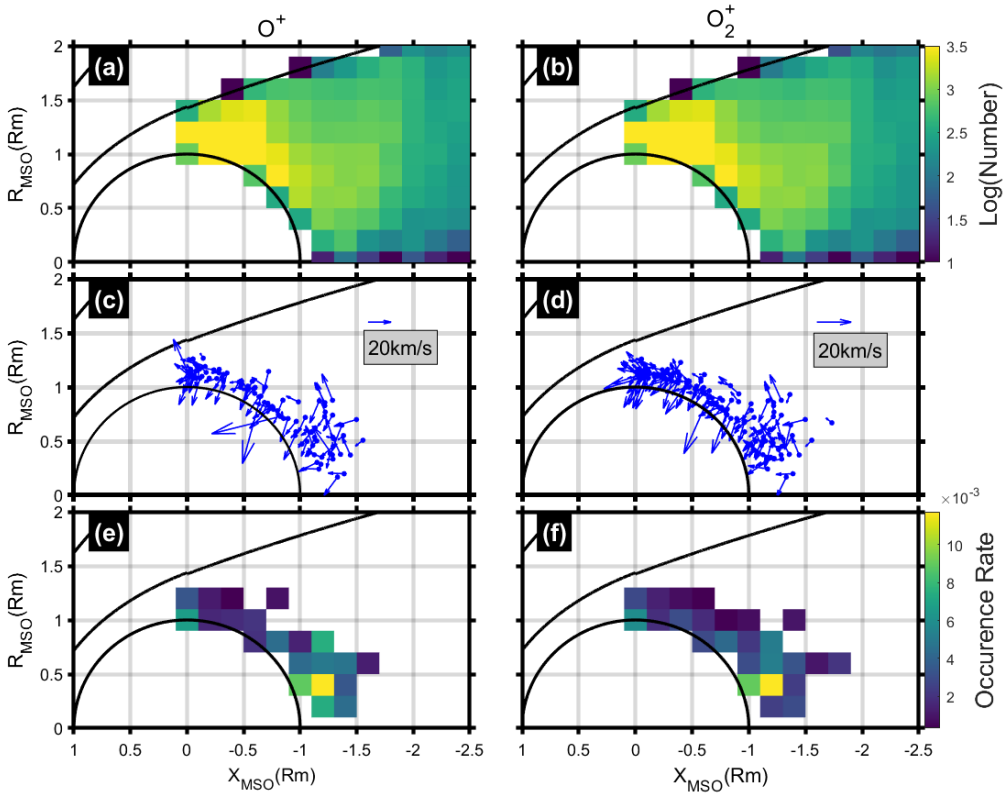

Figure 2. (a) and (b) show the total number of the data points with determined bulk velocity of O^+ and $O_2{}^+$ in XR_{MSO} plane. (c) and (d) display the projection of the bulk velocity of 98 events of sunward O^+ and 134 events of sunward $O_2{}^+$ respectively. (e) and (f) show the spatial occurrence rate of sunward O^+ and $O_2{}^+$ respectively. In all panels, black lines indicate the MPB, as found in the model of Trotignon et al. [2006], while black half-circles represent Mars.

We project the bulk velocity for 98 events of sunward O^+ and 134 events of sunward $O_2{}^+$ respectively onto the XR_{MSO} plane (Figures 2c and 2d). We find that the velocity of these events is mostly directed towards Mars, which confirms that the heavy ions are moving towards Mars; this suggests our selection criteria are valid.

Figures 2e and 2f show the spatial occurrence rate of sunward O^+ and $O_2{}^+$ respectively. This rate is calculated by $\frac{N_{\text{events}}}{N_{\text{total}}}$, where N_{events} represents the total sunward events and N_{total} the total number of data points in each spatial bin. The gaps or white region represent zero sunward flow events in that bin. Clearly, the spatial occurrence rate is higher near Mars (R_{MSO}<0.5Rm and X_{MSO}>–1.5Rm), whereas sunward flows disappear beyond X_{MSO}<–2Rm. Furthermore, the spatial occurrence rate is generally very low, with the largest value of 0.13 (Figure 2e–2f). This suggests that the appearance of sunward flows is scarce in

the Martian tail but more frequent in the Venusian tail [Persson et al., 2018].

1. Influence of Crustal Fields

In the case study discussed in Section 4, sunward flows occurred above the crustal fields, which might indicate that the flows are associated with crustal field. Here, we survey the spatial distribution of sunward flow events in Planetocentric coordinates to investigation the possible correlation with crustal fields.

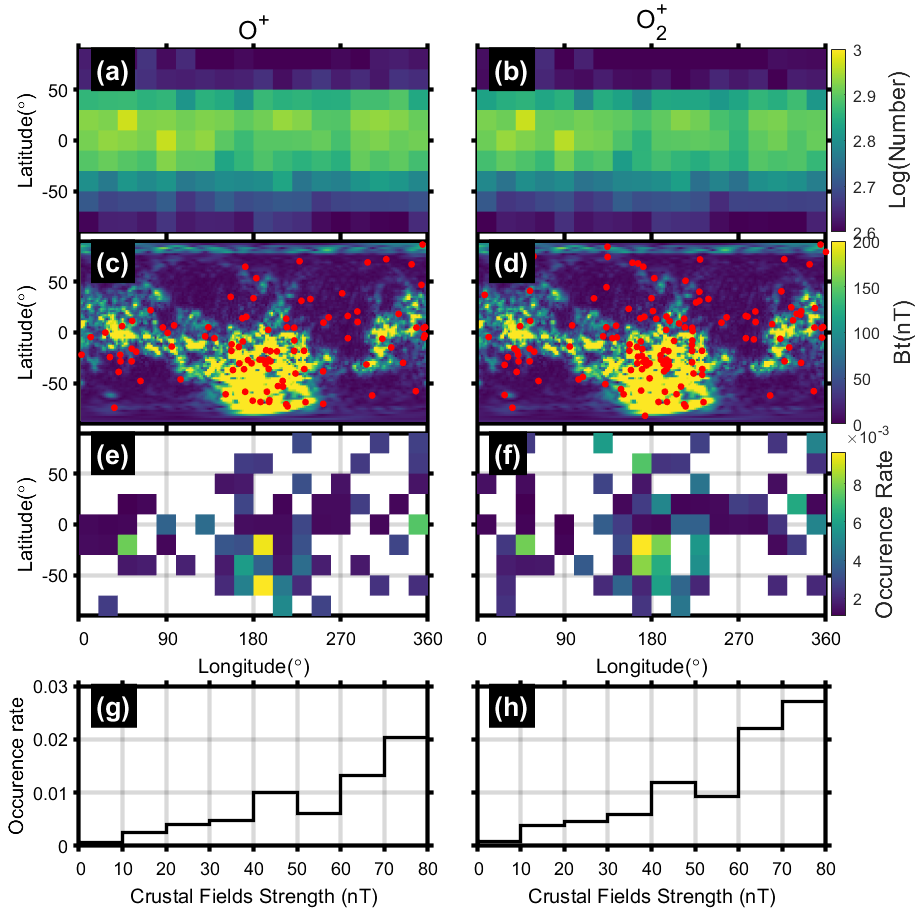

Figure 3. (a) and (b) show the map of total number of data points with determined bulk velocity of O^+ and $O_2{}^+$ respectively in Planetocentric coordinates. (c) and (d) display the locations of 98 events of sunward O^+ and 134 events of sunward $O_2{}^+$ respectively, which are represented by red dots overlapping a crustal fields model [Gao et al., 2021]. (e) and (f) show the spatial occurrence rate of sunward O^+ and $O_2{}^+$ respectively. (g) and (h) show the occurrence rate of sunward flows versus crustal magnetic fields strength respectively.

Figures 3a and 3b map the total number of data points with a determined bulk

velocity of O^+ and $O_2{}^+$ in each bin with a size of 20°×20° in Planetocentric coordinates. There are more observations near the equator region due to the bias of orbit coverage and the IMA's attitude. Figures 3c and 3d show the location of events of sunward O^+ and $O_2{}^+$ in Planetocentric coordinates that overlap with crustal fields at 160 km, which was obtained from a crustal fields model [Gao et al., 2021], respectively. Figure 3c–3f shows that most events for both O^+ and $O_2{}^+$ occurred above magnetic anomalies, especially in the strongest crustal fields region (Latitude~–50, Longitude~180).

Figure 3g–3h shows in greater detail the dependence between the occurrence frequency of sunward flows and the crustal fields' strength. Calculating the strength for each data point using the model of Gao et al. [2021], we find a clear correlation between crustal field strength and sunward O^+ and $O_2{}^+$. In the rightmost bin (80–90nT), the likelihood of sunward flow is nearly 2 to 3 times the planetary average (0.0077, 0.0107 for O^+, $O_2{}^+$).

These results strongly suggest that crustal fields play a key role in driving sunward flows. We also surveyed the relationship between these flows and the elevation angle of the crustal fields, but found no clear dependence (details not shown here). However, the low time resolution (192 s) of the IMA cannot resolve the fine structures of magnetic anomalies, which might affect this result.

1. Influence of Solar Activity

Kollmann et al. [2016] found that there is a correlation between Venusian sunward flows and solar activity. Our dataset covers over 13 years, corresponding to more than one solar cycle (one solar minimum to the next solar minimum), which provides an opportunity to investigate the relationship between sunward flows and solar activity at Mars.

Following the variations of the F10.7 index as shown in Figure 4a, we divide the data into three segments, which correspond to two solar minimum periods (green regions) and one solar maximum period (yellow region). Note that our results will not significantly be affected although the F10.7 index is measured at Earth.

From Figure 4b, we see that the temporal occurrence rate of both sunward O^+ and $O_2{}^+$ is higher during solar maximum, indicating a correlation with solar activity. This is similar to the case at Venus and implies that sunward flows might become more significant during solar maximum. However, the low temporal occurrence rate (on the order of 10^{-3} or 10^{-4}) of sunward flows indicates they do not dominate on Mars, regardless of the solar activity, while for Venus they can reach an occurrence rate as high as 0.8 [Kollmann et al., 2016].

To obtain the global response of sunward and tailward flux and its dependence on the solar activity, we follow Ramstad et al. [2015, 2018] and reconstruct the average ion distributions in the MSO frame for the period of each segment, where we re-binned the data into an average ion distribution by using an angular discretization step of $22.5^\circ \times 22.5^\circ$ and an energy table that is the same as the

post-2009 IMA one.

Based on the averaged ion distribution for the period of each segment, we can calculate the sunward flux, the tailward flux and the net flux for both O^+ and $O_2{}^+$ (Figures 4c–4e). Figures 4c and 4d show that the sunward flux is approximately two orders of magnitude lower than the tailward flux for the whole time, suggesting that tailward-escaping ions were dominating regardless of solar activity. Furthermore, although the sunward flux reaches higher levels during solar maximum (Figure 4c), the more enhanced tailward flux (Figure 4d) leads to an increased net escape of ions (Figure 4e), which is different to the case at Venus where the net escape is reduced during solar maximum. Our results are also consistent with previous studies that positively correlate net escape and solar activity at Mars [e.g., Ramstad et al., 2015; Dubinin et al., 2017; Dong et al., 2017; Nilsson et al., 2021].

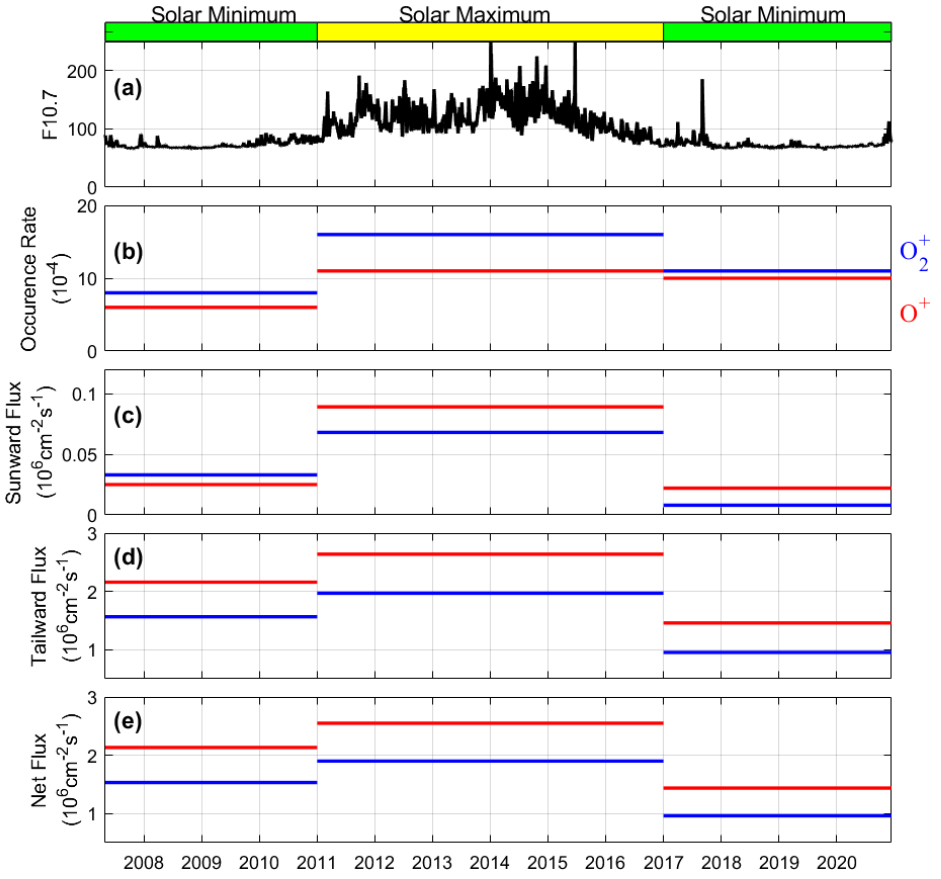

Figure 4. (a) F10.7 index; (b) temporal occurrence rate of sunward O^+ (red) and $O_2{}^+$ (blue); (c), (d), and (e) show the sunward, tailward and net flux of O^+ and $O_2{}^+$, respectively. The green (yellow) shadow regions above this figure

represent the time interval of solar minimum (solar maximum).

1. Discussion and Conclusion

Using over 13 years of ion data that was measured by the IMA onboard Mars Express, we performed a statistical survey on sunward flows of heavy ions (O^+ and $O_2{}^+$) in the Martian magnetotail. Our study provides a global picture of such sunward flows, which could help us understand plasma dynamics and ion escape at Mars. The main results can be summarized as follows:

1. Both the sunward O^+ and $O_2{}^+$ mainly occur around crustal fields and are associated with strong crustal fields, indicating that they play a key role in generating sunward flows.
2. During solar maximum, as opposed to solar minimum, the temporal occurrence rate of sunward flows increases and the sunward flux is higher. However, more enhanced tailward flux still leads to greater ion removal during solar maximum.
3. The temporal occurrence rate of sunward flows (on the order of 10^{-3} to 10^{-4}) are low regardless of solar activity. Furthermore, the sunward flux is about two orders of magnitude lower than the tailward flux, indicating that most of the heavy ions were escaping to interplanetary space rather than returning to Mars. This result suggests that sunward flows will not reduce the ion escape significantly at Mars during any solar activities, which is different in the case at Venus.

In terms of the space environment, there are three major differences between Venus and Mars. The first is that plasma dynamics on Mars are more kinetic than those on Venus due to the small radius of Mars. Compared with the significant presence of sunward flows at Venus, our results might suggest that kinetic effects (e.g., the finite gyroradius effect) inhibit the generation of these flows. The second is that the plasma density of the Martian ionosphere is far more tenuous than that of the Venusian ionosphere. Thus, the draped field lines in the Martian tail could move faster due to a weaker mass-loading effect of the ionosphere; this could inhibit magnetic energy storage and the triggering of magnetic reconnections in the tail. As a result, sunward flows triggered by such reconnection would be seldom observed. However, during solar maximum, the ionosphere becomes denser and broader and forms a more Venus-like environment, which could increase the occurrence rate of sunward flows [e.g., Yamauchi et al., 2015; Liemohn et al., 2017].

The third difference is that Mars possess localized intense crustal fields. The crustal fields can trap tailward heavy ions, forming the sunward flows that even return to Mars. In addition, non-gyrotropic distribution of ions driven by the crustal fields could sometimes manifest as a sunward flow. For example, when the ions gyrate downward into strong crustal fields, on the assumption they are below the altitude of spacecraft, these ions cannot move back towards the spacecraft's location due to a significant decrease of gyroradius ($\frac{\mathrm{mV}}{\mathrm{Bq}}$): that is,

they are trapped by crustal fields below spacecraft altitude. This may lead to the sunward flows that we observed. This might explain the correlation between crustal fields and sunward flows, as well as there being no dependence on the local elevation angle of crustal fields (since strong ones are below the altitude of spacecraft). However, this mechanism is only valid for sunward flows that occurred at a distance between crustal fields and locations shorter than 2×gyroradius.

For sunward flows that occurred at a high altitude, we suggest that they are a results of tail reconnection and sunward J×B force [e.g., Zhang et al., 2012; Gao et al., 2021; Harada et al., 2015b, 2017, 2020; Zhang et al., 2022]. Therefore, a combination of several mechanisms might drive sunward flows at Mars. We also find that sunward flows only occur in the near-tail (X_{MSO}>-2R_m). If reconnection could drive sunward flows, our results imply that magnetic reconnection cannot occur in the distant tail (X_{MSO}<-2R_m). This is consistent with the study of Harada et al. [2017, 2020].

Data Availability Statement

The ASPERA-3 IMA data used, the case we studied, and the selected events are public in the Zenodo repository (https://doi.org/10.5281/zenodo.6952674) [Zhang, 2022]. The F10.7 index was retrieved through the OMNI data service at https://omniweb.gsfc.nasa.gov.

Acknowledgments

This work is supported by the National Natural Science Foundation of China (grants 41922031, 41774188), the Strategic Priority Research Program of Chinese Academy of Sciences (Grant No. XDA17010201, XDB41000000), the Key Research Program of Chinese Academy of Sciences (Grant No. ZDBS-SSW-TLC00103), and the Key Research Program of the Institute of Geology & Geophysics, CAS (Grant No. IGGCAS- 201904, IGGCAS- 202102). Chi Zhang is supported by China Scholarship Council (Student Number. 202104910297). We thank Yuki Harada, Jiawei Gao, Zhen Shi and Xinzhou Li for their helpful discussion.

References

Barabash, S., Dubinin, E., Pissarenko, N., Lundin, R., & Russell, C. T. (1991). Picked-up protons near Mars: Phobos observations. Geophysical Research Letters, 18(10), 1805-1808.

Barabash, S., et al. (2006), The Analyzer of Space Plasma and Energetic Atoms (ASPERA-3) for the Mars Express mission, Space Sci. Rev., 126, 113.

Barabash, S., Fedorov, A., Lundin, R., & Sauvaud, J.-A. (2007). Martian Atmospheric Erosion Rates. Science, 315(5811), 501–503.

Bergman, S., Stenberg Wieser, G., Wieser, M., Johansson, F. L., & Eriksson, A. (2020). The influence of spacecraft charging on low-energy ion measurements

made by RPC-ICA on Rosetta. Journal of Geophysical Research: Space Physics, 125(1), e2019JA027478.

Brain, D. A., McFadden, J. P., Halekas, J. S., Connerney, J. E. P., Bougher, S. W., Curry, S., ... & Seki, K. (2015). The spatial distribution of planetary ion fluxes near Mars observed by MAVEN. Geophysical Research Letters, 42(21), 9142-9148.

Collinson, G., Glocer, A., Xu, S., Mitchell, D., Frahm, R. A., Grebowsky, J., ... & Jakosky, B. (2019). Ionospheric ambipolar electric fields of Mars and Venus: Comparisons between theoretical predictions and direct observations of the electric potential drop. Geophysical research letters, 46(3), 1168-1176.

Connerney, J. E. P., Acuña, M. H., Ness, N. F., Kletetschka, G., Mitchell, D. L., Lin, R. P., & Rème, H. (2005). Tectonic implications of Mars crustal magnetism. Proceedings of the National Academy of Sciences of the United States of America, 102(42), 14970–14975. https://doi. org/10.1073/pnas.0507469102

Diéval, C., G. Stenberg, H. Nilsson, and S. Barabash (2013), A statistical study of proton precipitation onto the Martian upper atmosphere: Mars Express observations, J. Geophys. Res. Space Physics, 118, 1972–1983, doi:10.1002/jgra.50229.

Dong, C., S. W. Bougher, Y. Ma, G. Toth,A. F. Nagy, and D. Najib (2014), Solarwind interaction with Mars upperatmosphere: Results from the one-waycoupling between the multifluidMHD model and the MTGCM model,Geophys. Res. Lett.,41, 2708–2715,doi:10.1002/2014GL059515

Dong, C., S. W. Bougher, Y. Ma,G. Toth, Y. Lee, A. F. Nagy, V. Tenishev,D. J. Pawlowski, M. R. Combi, and D.Najib (2015), Solar wind interactionwith the Martian upper atmosphere:Crustal field orientation, solar cycle,and seasonal variations,J. Geophys.Res. Space Physics,120, 7857–7872,doi:10.1002/2015JA020990

Dong, Y., Fang, X., Brain, D. A., McFadden, J. P., Halekas, J. S., Connerney, J. E. P., ... & Jakosky, B. M. (2017). Seasonal variability of Martian ion escape through the plume and tail from MAVEN observations. Journal of Geophysical Research: Space Physics, 122(4), 4009-4022.

Dong, Y., Fang, X., Brain, D. A., McFadden, J. P., Halekas, J. S., Connerney, J. E., ... & Jakosky, B. M. (2015). Strong plume fluxes at Mars observed by MAVEN: An important planetary ion escape channel. Geophysical Research Letters, 42(21), 8942-8950.

Dubinin, E., Fraenz, M., Fedorov, A., Lundin, R., Edberg, N., Duru, F., & Vaisberg, O. (2011). Ion Energization and Escape on Mars and Venus. Space Science Reviews, 162(1), 173–211.

Dubinin, E., Fraenz, M., Pätzold, M., McFadden, J., Mahaffy, P. R., Eparvier, F., ... & Zelenyi, L. (2017). Effects of solar irradiance on the upper ionosphere

and oxygen ion escape at Mars: MAVEN observations. Journal of Geophysical Research: Space Physics, 122(7), 7142-7152.

Dubinin, E., Fraenz, M., Woch, J., Zhang, T. L., Wei, J., Fedorov, A., ... & Lundin, R. (2012). Bursty escape fluxes in plasma sheets of Mars and Venus. Geophysical Research Letters, 39(1).

Dubinin, E., Fraenz, M., Zhang, T. L., Woch, J., Wei, Y., Fedorov, A., ... & Lundin, R. (2013). Plasma in the near Venus tail: Venus Express observations. Journal of Geophysical Research: Space Physics, 118(12), 7624-7634.

Fang, X., Liemohn, M. W., Nagy, A. F., Luhmann, J. G., & Ma, Y. (2010). On the effect of the Martian crustal magnetic field on atmospheric erosion. Icarus, 206(1), 130-138.

Fang, X., Liemohn, M. W., Nagy, A. F., Ma, Y., De Zeeuw, D. L., Kozyra, J. U., & Zurbuchen, T. H. (2008). Pickup oxygen ion velocity space and spatial distribution around Mars. Journal of Geophysical Research: Space Physics, 113(A2).

Fedorov, A., Barabash, S., Sauvaud, J. A., Futaana, Y., Zhang, T. L., Lundin, R., & Ferrier, C. (2011). Measurements of the ion escape rates from Venus for solar minimum. Journal of Geophysical Research: Space Physics, 116(A7).

Fränz, M., Dubinin, E., Andrews, D., Barabash, S., Nilsson, H., & Fedorov, A. (2015). Cold ion escape from the Martian ionosphere. Planetary and Space Science, 119, 92-102.

Fränz, M., Dubinin, E., Roussos, E., Woch, J., Winningham, J. D., Frahm, R., ... & Lundin, R. (2007). Plasma moments in the environment of Mars. In The Mars Plasma Environment (pp. 165-207). Springer, New York, NY.

Futaana, Y. , Wieser, G. S. , Barabash, S. , & Luhmann, J. G. . (2017). Solar wind interaction and impact on the venus atmosphere. Space Science Reviews.

Gao, J. W., Rong, Z. J., Persson, M., Stenberg, G., Zhang, Y. C., Klinger, L., ... & Futaana, Y. (2021). In situ observations of the ion diffusion region in the Venusian magnetotail. Journal of Geophysical Research: Space Physics, 126(1), e2020JA028547.

Gao, J.W., Rong, Z.J., Klinger Lucy, Li, X.Z., Liu, D., Wei, Y. (2021). A spherical harmonic Martian crustal magnetic field model combining data sets of MAVEN and MGS, Earth and Space Science, doi: 10.1029/2021EA001860.

Hara, T., Luhmann, J. G., Leblanc, F., Curry, S. M., Halekas, J. S., Seki, K., et al. (2018). Evidence for crustal magnetic field control of ions precipitating into the upper atmosphere of Mars. Journal of Geophysical Research: Space Physics, 123, 8572–8586. https://doi.org/10.1029/2017JA024798

Harada, Y., Halekas, J. S., McFadden, J. P., Espley, J., DiBraccio, G. A., Mitchell, D. L., ... & Jakosky, B. M. (2017). Survey of magnetic reconnection

signatures in the Martian magnetotail with MAVEN. Journal of Geophysical Research: Space Physics, 122(5), 5114-5131.

Harada, Y., Halekas, J. S., McFadden, J. P., Mitchell, D. L., Mazelle, C., Connerney, J. E. P., ... & Jakosky, B. M. (2015a). Marsward and tailward ions in the near-Mars magnetotail: MAVEN observations. Geophysical Research Letters, 42(21), 8925-8932.

Harada, Y., Halekas, J. S., McFadden, J. P., Mitchell, D. L., Mazelle, C., Connerney, J. E. P., ... & Jakosky, B. M. (2015b). Magnetic reconnection in the near-Mars magnetotail: MAVEN observations. Geophysical Research Letters, 42(21), 8838-8845.

Harada, Y., Halekas, J. S., Xu, S., DiBraccio, G. A., Ruhunusiri, S., Hara, T., ... & Mazelle, C. (2020). Ion jets within current sheets in the Martian magnetosphere. Journal of Geophysical Research: Space Physics, 125(12), e2020JA028576.

Inui, S., Seki, K., Sakai, S., Brain, D. A., Hara, T., McFadden, J. P., et al. (2019). Statistical study of heavy ion outflows from Mars observed in the Martian-induced magnetotail by MAVEN. Journal of Geophysical Research: Space Physics, 124, 5482–5497. https://doi.org/10.1029/ 2018JA026452

Kollmann, P., Brandt, P. C., Collinson, G., Rong, Z. J., Futaana, Y., & Zhang, T. L. (2016). Properties of planetward ion flows in Venus' magnetotail. Icarus, 274, 73-82.

Liemohn, M. W., Xu, S., Dong, C., Bougher, S. W., Johnson, B. C., Ilie, R., & De Zeeuw, D. L. (2017). Ionospheric control of the dawn-dusk asymmetry of the Mars magnetotail current sheet. Journal of Geophysical Research: Space Physics, 122(6), 6397-6414.

Luhmann, J. G., S. A. Ledvina, and C. T. Russell (2004), Induced magnetospheres, Adv. Space Res., 33, 1905–1912.

Lundin, R. (2011). Ion acceleration and outflow from Mars and Venus: An overview. The plasma environment of Venus, Mars, and Titan, 309-334.

Lundin, R., Zakharov, A., Pellinen, R., Borg, H., Hultqvist, B., Pissarenko, N., ... & Koskinen, H. (1989). First measurements of the ionospheric plasma escape from Mars. Nature, 341(6243), 609-612.

Ma, Y. J., Dong, C. F., Toth, G., van der Holst, B., Nagy, A. F., Russell, C. T., ... & Jakosky, B. M. (2019). Importance of ambipolar electric field in driving ion loss from Mars: Results from a multifluid MHD model with the electron pressure equation included. Journal of Geophysical Research: Space Physics, 124(11), 9040-9057.

Ma, Y., Nagy, A. F., Hansen, K. C., DeZeeuw, D. L., Gombosi, T. I., & Powell, K. (2002). Three-dimensional multispecies MHD studies of the solar wind

interaction with Mars in the presence of crustal fields. Journal of Geophysical Research, 107(A10), 1282–1289.

Masunaga, K., Futaana, Y., Persson, M., Barabash, S., Zhang, T. L., Rong, Z. J., & Fedorov, A. (2019). Effects of the solar wind and the solar EUV flux on O+ escape rates from Venus. Icarus, 321, 379-387.

Nilsson, H., Carlsson, E., Brain, D. A., Yamauchi, M., Holmström, M., Barabash, S., ... & Futaana, Y. (2010). Ion escape from Mars as a function of solar wind conditions: A statistical study. Icarus, 206(1), 40-49.

Nilsson, H., Edberg, N. J. T., Stenberg, G., Barabash, S., Holmström, M., Futaana, Y., … Fedorov, A. (2011). Heavy ion escape from Mars, influence from solar wind conditions and crustal magnetic fields. Icarus, 215(2), 475–484.

Nilsson, H., Stenberg, G., Futaana, Y., Holmström, M., Barabash, S., Lundin, R., ... & Fedorov, A. (2012). Ion distributions in the vicinity of Mars: Signatures of heating and acceleration processes. Earth, planets and space, 64(2), 135-148.

Nilsson, H., Zhang, Q., Wieser, G. S., Holmström, M., Barabash, S., Futaana, Y., … Wieser, M. (2021). Solar cycle variation of ion escape from Mars. Icarus, 114610.

Persson, M., Futaana, Y., Fedorov, A., Nilsson, H., Hamrin, M., & Barabash, S. (2018). H+/O+ escape rate ratio in the Venus magnetotail and its dependence on the solar cycle. Geophysical Research Letters, 45(20), 10-805.

Persson, M., Futaana, Y., Ramstad, R., Masunaga, K., Nilsson, H., Hamrin, M., ... & Barabash, S. (2020). The Venusian atmospheric oxygen ion escape: Extrapolation to the early solar system. Journal of Geophysical Research: Planets, 125(3), e2019JE006336.

Ramstad, R., Barabash, S., Futaana, Y., Nilsson, H., & Holmström, M. (2018). Ion escape from Mars through time: an extrapolation of atmospheric loss based on 10 years of Mars Express measurements. Journal of Geophysical Research: Planets, 123(11), 3051-3060.

Ramstad, R., Barabash, S., Futaana, Y., Nilsson, H., Wang, X. D., & Holmström, M. (2015). The Martian atmospheric ion escape rate dependence on solar wind and solar EUV conditions: 1. Seven years of Mars Express observations. Journal of Geophysical Research: Planets, 120(7), 1298-1309.

Rojas-Castillo, D., Nilsson, H., & Stenberg Wieser, G. (2018). Mass composition of the escaping flux at Mars: MEX observations. Journal of Geophysical Research: Space Physics, 123(10), 8806-8822.

Trotignon, J. G., Mazelle, C., Bertucci, C., & Acuña, M. H. (2006). Martian shock and magnetic pile-up boundary positions and shapes determined from the Phobos 2 and Mars Global Surveyor data sets. Planetary and Space Science, 54(4), 357–369.

Voshchepynets, A., Barabash, S., Ramstad, R., Holmstrom, M., Andrews, D., Nicolaou, G., ... & Gurnett, D. (2018). Ions Accelerated by Sounder-Plasma Interaction as Observed by Mars Express. Journal of Geophysical Research: Space Physics, 123(11), 9802-9814.

Xu, S., Mitchell, D. L., Ma, Y., Weber, T., Brain, D. A., Halekas, J., ... & Mazelle, C. (2021). Global Ambipolar Potentials and Electric Fields at Mars Inferred From MAVEN Observations. Journal of Geophysical Research: Space Physics, 126(12), e2021JA029764.

Yamauchi, M., Hara, T., Lundin, R., Dubinin, E., Fedorov, A., Sauvaud, J. A., ... & Barabash, S. (2015). Seasonal variation of Martian pick-up ions: Evidence of breathing exosphere. Planetary and Space Science, 119, 54-61.

Zhang, C., Rong, Z. J., et al. (2021). MAVEN Observations of Periodic Low-altitude Plasma Clouds at Mars. The Astrophysical Journal Letters, 922, L33. https://doi.org/10.3847/2041-8213/ac3a7d

Zhang, C., Rong, Z. J., et al. (2022). Three-dimensional Configuration of Induced Magnetic Fields around Mars. Journal of Geophysical Research: Planets, under review. Doi: 2022JE007334.

Zhang. C. (2022). Supporting data for_Sunward Ion Flows in the Martian Magnetotail: Mars Express Observations [Data set]. Zenodo. https://doi.org/10.5281/zenodo.6952674.

Zhang, T. L., Lu, Q. M., Baumjohann, W., Russell, C. T., Fedorov, A., Barabash, S., ... & Balikhin, M. (2012). Magnetic reconnection in the near Venusian magnetotail. Science, 336(6081), 567-570.